

RESEARCH ARTICLE

10.1002/2017JD026460

Key Points:

- Anvil cloud properties determine the radiation balance in the convective tropics
- The effect of tropical clouds on the energy balance depends on the distribution of anvil cloud optical depth
- Anvil cloud radiative interactions influence anvil cloud properties

Correspondence to:

D. L. Hartmann,
dhartm@u.washington.edu

Citation:

Hartmann, D. L., and Berry, S. E. (2017), The balanced radiative effect of tropical anvil clouds, *J. Geophys. Res. Atmos.*, 122, doi:10.1002/2017JD026460.

Received 5 JAN 2017

Accepted 13 APR 2017

Accepted article online 19 APR 2017

The balanced radiative effect of tropical anvil clouds

Dennis L. Hartmann¹  and Sara E. Berry¹ ¹Department of Atmospheric Sciences, University of Washington, Seattle, Washington, USA

Abstract Coincident instantaneous broadband radiation budget measurements from Clouds and Earth's Radiant Energy System and cloud vertical structure information from CloudSat-Cloud-Aerosol Lidar and Infrared Pathfinder Satellite Observations radar-lidar observations are combined to study the relationship of cloud vertical structure to top-of-atmosphere energy balance fluctuations. Varying optical and physical thickness of high ice clouds produces most of the covariation between albedo and outgoing longwave radiation in regions of tropical convection. Rainy cores of tropical convective clouds have a negative impact on the radiation balance, while nonprecipitating anvil clouds have a positive effect. The effect of anvil clouds on the radiative heating profile is to warm near cloud base and cool near cloud top, and to reduce the radiative cooling rate in the clear air below the cloud. The cooling rate in the clear air below the anvil is reduced to small values for moderately thick anvils, and the driving of instability in the anvil itself also saturates for relatively thin clouds. It is hypothesized that the dependence of radiative heating on cloud thickness may be important in driving the distribution of tropical cloud structures toward one that produces net neutrality of the cloud radiative effect at the top-of-the-atmosphere, as is found in regions of deep convection over ocean areas with high and relatively uniform surface temperatures. This idea is tested with a single-column model, which indicates that cloud-radiation interactions affect anvil cloud properties, encouraging further investigation of the hypothesis.

Plain Language Summary Satellite data are used to show that tropical convective clouds have a small net effect on the energy balance because the cooling effect of thick tropical clouds is offset by the warming effect of thin upper level clouds that are connected to the thick clouds. Why these two types of clouds cancel each other out nearly exactly in the warm regions of the tropics is unknown. The effect of radiative transfer on the anvil clouds seems to be a possible contributor to the abundance of thin high clouds that give the positive influences on the radiation budget at the top of the atmosphere.

1. Introduction

It has long been observed that the net radiation in cloudy regions of the convective tropics is virtually the same as the net radiation in nearby nonconvective regions, despite the fact that the average longwave and shortwave cloud radiative effects of deep convective cloud are both large [Harrison *et al.*, 1990; Hartmann and Short, 1980; Ramanathan *et al.*, 1989]. Figure 1 shows the longwave (LWCRE), shortwave (SWCRE), and Total (TotalCRE) cloud radiative effects for the June through August season from the Clouds and Earth's Radiant Energy System (CERES) [Wielicki *et al.*, 1996]. Over the Indian Ocean to western Pacific Ocean region near the equator, the TotalCRE is small, while the LWCRE and SWCRE are each large but tend to cancel each other. The large longwave trapping by the high clouds in the tropics in these regions is cancelled very closely by the amount of additional solar radiation that these clouds reflect, so that the pattern of high cloud abundance that is obvious in the LWCRE is not apparent in the pattern of TotalCRE. As long as the high clouds have this aggregate net neutrality their effect on the large-scale climate is mostly limited to flattening the sea surface temperature (SST) distribution in the warm pool areas [Peters and Bretherton, 2005]. It is an important question whether this shortwave-longwave top-of-atmosphere balance in the radiative effect of tropical clouds results from a coincidence such that these features of tropical clouds might change in a warmed world, or whether feedback processes exist to maintain this condition in an altered climate. The answer might have an important impact on climate sensitivity. Kiehl [1994] argued that the cancellation is a result of the tropopause temperature and that tropical convective clouds are optically thick in both the infrared and solar wavelengths. Hartmann *et al.* [2001] argued that tropical convective clouds range from optically thin to optically thick, and have a wide range of effects on the radiation balance, so that some other logic may be needed to explain the cancellation of the large longwave and shortwave effects of clouds on the radiation balance. They proposed a negative

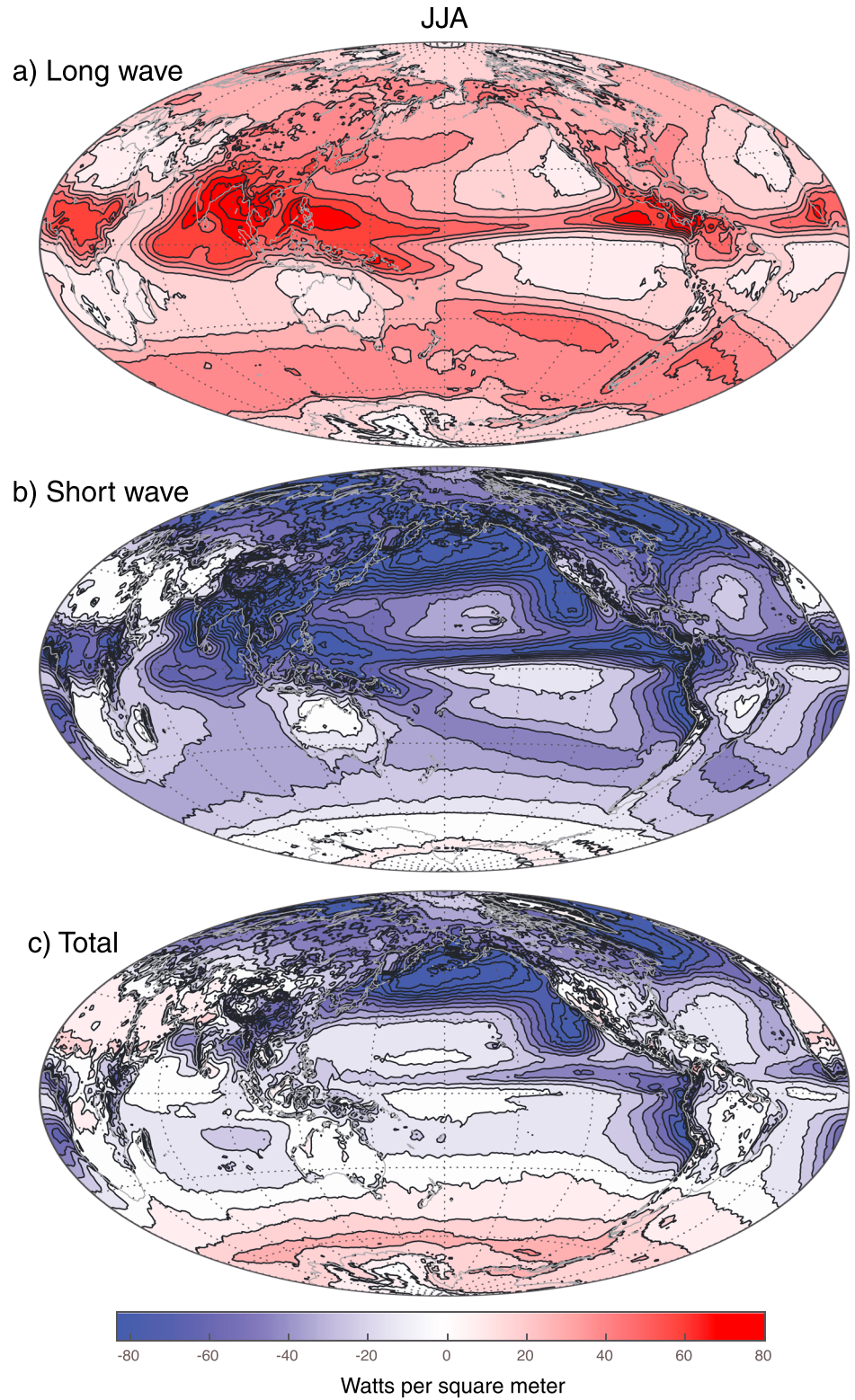


Figure 1. (a) Longwave, (b) shortwave and (c) total cloud radiative effects during June-July-August from CERES measurements for 2000–2013. Contour interval is 10 W m^{-2} . Hammer projection centered on 180°E .

feedback mechanism whereby a positive net radiation anomaly leads to convection, which increases the albedo of convective clouds until the net radiation is reduced to that of the surrounding convection-free atmosphere. Conversely, a negative net radiation anomaly would suppress convection and lead to thinner clouds and also drive the net radiation back to a value that is uniform across the region of convection and nearby clear skies. The cloud top temperature is maintained around 220 K according to the Fixed Anvil Temperature Hypothesis [Hartmann and Larson, 2002], so that the cloud thickness adjustment would mostly affect the albedo, rather than the OLR.

Hartmann *et al.* [2001] developed a simple model that would produce this strong negative feedback and maintain a constant net radiation, but it has not been verified observationally or with more complete models. Moreover, the adjustment seems to take place rapidly in nature, without an observable effect on SST, so it seems promising to look for feedback mechanisms that operate within the atmosphere on time scales that are comparable to the lifetime of convective clouds. In this paper we look at observations of the vertical structure of tropical convective clouds in reference to their top-of-atmosphere (TOA) radiative effects using collocated CERES and Cloudsat-Cloud-Aerosol Lidar and Infrared Pathfinder Satellite Observations (CALIPSO) data. We then do some calculations to illustrate the effect of these layers on radiative heating of the atmosphere. These results suggest that elevated clouds of intermediate optical depth may be favored by the atmospheric radiative heating that they produce. This idea is then tested in a single-column model by comparing the behavior of ice clouds with and without the cloud radiative effects included.

Houze [1982] showed that the radiative heating and cooling associated with upper level stratiform cloud is almost as important as that associated with the convective towers and the stratiform precipitation processes, and that the radiative heating contributed to raising the altitude of the maximum vertical velocity in the convective tropics. The effect of radiation on high tropical cloud layers has also been investigated by Ackerman *et al.* [1988], who showed that heating rates in tropical cloud anvils can be very large, with heating at the bottom and cooling at the top for thicker clouds, and that this heating is dominated by longwave radiation. They inferred that heating of anvil clouds could have a large effect on large-scale climate as well as the anvils themselves. They also note that as the clouds become deeper, with a lower cloud base, the radiative heating of the cloud layer decreases.

Fu *et al.* [1995] used a two-dimensional cumulus ensemble model to show that fully interactive longwave radiative heating destabilizes anvil clouds and contributes to their longevity and horizontal extent. The interaction of the radiative heating of tropical cirrus with atmospheric dynamics was recently considered by Harrop and Hartmann [2016], who showed that in a cloud-resolving model the radiative heating anomalies associated with the presence of cirrus clouds tend to increase the area coverage of anvil clouds and also reduce the average optical depth of anvil clouds, decreasing the shortwave cloud effect relative to the longwave cloud effect. They also showed that kinetic energy in the cloud layer is enhanced when the radiative effects of the cloud are included, indicating that motion fields are enhanced by the radiative interactions. This is consistent with lifting of thin clouds near the tropical tropopause by radiative heating of the layers and generation of an associated circulation, as shown by Lilly [1988], Durran *et al.* [2009], and Dinh *et al.* [2010]. For thicker clouds, longwave radiation heats the cloud layer at its base and cools the cloud layer at its top, thus generating instability in the cloud layer as well as net heating in the cloud layer.

In section 2 we look at the vertical structure of clouds in the convective tropics where a large cancellation between longwave and shortwave cloud radiative effects occurs. We relate the vertical structure as measured by CloudSat-CALIPSO to the albedo-OLR histogram measured by CERES. In section 3 radiative transfer calculations are done to show that the albedo-OLR histogram structure can be explained simply with tropical anvil cloud structure of varying physical and optical thickness and nearly constant top altitude. These calculations also indicate a strong role for radiation in determining the abundance and structure of anvil clouds. We then hypothesize that the radiative driving associated with elevated anvil clouds may play a key role in driving the average optical depth toward a value that roughly cancels the longwave effect of the clouds. Section 4 illustrates that the structure of radiative heating calculated from the observed clouds is similar to hypothetical clouds considered in section 3. In section 5 the response of anvil-like ice clouds to their radiative heating is tested with a single-column model. A summary and conclusion is presented in section 6.

2. Cloud Structure and Radiation Budget Data

We use the CALIPSO-CloudSat-CERES-MODIS (CCCM) data set, which integrates measurements from the Cloud-Aerosol Lidar and Infrared Pathfinder Satellite Observations (CALIPSO), Cloud-Aerosol Lidar with Orthogonal Polarization (CALIOP), CloudSat Cloud Profiling Radar (CPR), Clouds and the Earth's Radiant Energy System (CERES), and the Moderate Resolution Imaging Spectroradiometer (MODIS) data. These data were obtained from the Langley Atmospheric Sciences Data Center and have the data designator CER-NEWS_CCCM_Aqua-FM3-MODIS-CAL-CS_ReIB1. The cloud and aerosol properties from CALIOP and cloud properties from the CPR are matched to a MODIS pixel and then an Aqua CERES footprint. The data set contains only the CERES footprint in each scan that has the highest CALIPSO and CloudSat ground track coverage. We will focus on the CERES measurements of broadband albedo and outgoing longwave radiation [Wielicki *et al.*, 1996], and the cloud layer data from the combined CloudSat and CALIOP data [Mace *et al.*, 2009; Stephens *et al.*, 2008; Winker *et al.*, 2009; Winker *et al.*, 2010]. These data together will allow an examination of the relationship between tropical cloud vertical structure and the (TOA) radiation balance.

Active profiling of tropical convective clouds with the CloudSat cloud profiling radar and the CALIPSO cloud-aerosol lidar has provided new information on the structure of tropical convective cloud complexes. Yuan and Houze [2010] and Yuan *et al.* [2011] used coincident satellite measurements of 11 μm longwave emission, precipitation from microwave imaging, and CloudSat radar returns to investigate the structure of mesoscale convective systems in the tropics and the associations among convective cores, surrounding regions of light precipitation, and the anvil clouds attached to them that thin out with distance from the regions of heavy rainfall. Yuan and Houze [2013] found that increased precipitation, more connected mesoscale convective systems, and a more humid midtroposphere were strongly related. They found that the larger connected systems produced less, but colder anvil cloud. Igel *et al.* [2014] used CloudSat data to define tropical cloud objects consisting of a pedestal and an anvil, counted the number of convective cores within each pedestal, and measured the extent of the anvil from the pedestal as a function of SST. Deng *et al.* [2016] further investigated the structure of mesoscale convective systems using a different classification system applied to CloudSat and CALIPSO data and found that the anvil ice mass per unit volume of the whole cluster levels off as the scale of the cluster passes 200 km, but the anvil volume keeps increasing as the scale increases, implying enhanced production of thin anvil cloud for larger systems. These remote sensing measurements give quantitative, global data on the classic morphology of tropical convective complexes as consisting of convective cores, connected to regions of stratiform precipitation from anvil clouds, connected to nonprecipitating anvils that thin as they spread outward from convection and persist after the active convection ceases.

Berry and Mace [2014] used CloudSat/CALIPSO data to determine the properties of clouds in Southeast Asia during the rainy season. They calculated the radiative effects of these clouds and found that abundant thin ice clouds produced a warming effect at the top of the atmosphere, while thicker rainy clouds produced a negative effect on the radiation balance. They showed that the mean value of ice content is not useful in calculating the radiative effects of clouds, but that the whole distribution of clouds is important, especially clouds with the median ice content, which is relatively low. The work presented here will draw similar conclusions for convection in the West Pacific but present the data in a different way.

To sample a region in which CERES data show that the longwave and shortwave cloud radiative effects are approximately in balance, we choose the Western Equatorial Pacific region (12°N–12°S, 150°E–170°E) and use all the data for July through August 2006–2010. We select CERES pixels for which the solar zenith angle and the CERES viewing zenith are both less than 40°. Since the Aqua satellite and other A-Train instruments used for the CCCM data set are in a 1:30 P.M. Sun-synchronous orbit, and CloudSat/CALIOP is nadir staring, this mostly limits the observations to daytime when the albedo can be measured. We have looked at other convective regions in the tropics such as the Indian Ocean during summer and found very similar results, with only minor variations in the cloud structure indicated here, so that we feel these results are characteristic of oceanic convective regions in the tropics where the SST is warm and relatively uniform. The convective cloud structure is different in the eastern tropical Pacific ITCZ region, where less anvil and more boundary layer cloud are present, as shown by Kubar *et al.* [2007] and Yuan and Houze [2010].

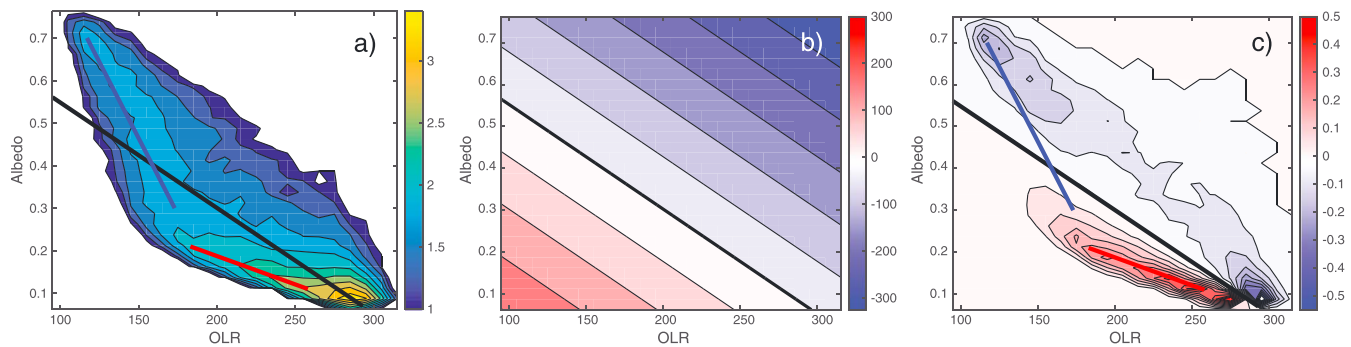


Figure 2. (a) Histogram of CERES CCCM footprint albedo and OLR pairings for the equatorial western Pacific Ocean region. The contours are \log_{10} of counts in 10 W m^{-2} OLR, by 0.025 albedo bins. (b) Net TOA radiation contrast between clouds with different albedos and OLRs compared with the modal values 0.08 and 289 W m^{-2} , respectively. Contour interval is 50 W m^{-2} , and the heavy black line indicates zero difference from the modal values. (c) Product of the fractional abundance of clouds in each albedo-OLR bin, from Figure 2a, and the net radiative effect of clouds in that bin, compared to the ‘modal value’ value, as shown in Figure 2b. The contours in Figure 2c indicate the relative contribution of different albedo-OLR pairings to the net radiation anomaly from the modal value. See text for further details.

2.1. Cloud Histograms and Cloud Radiative Effects

Figure 2a shows the two-dimensional histogram of CERES footprint OLR and albedo for the selected region and time. The mean albedo and OLR for this region are 20.5% and 231 W m^{-2} , respectively. Most clouds are either dimmer and warmer, or brighter and colder than this, so the mean values are not typical. The histogram is dominated by a large number of scenes with an OLR of around 289 W m^{-2} and an albedo of about 8% , which we will call the modal point of the histogram, but which also corresponds to nearly clear skies. The difference in net radiation at TOA between this most common scene and the average scene is less than 5 W m^{-2} , so that the average impact of the convective clouds on the TOA radiation balance is very small. The black line in Figure 2 passes through the modal point and the other points in the histogram that have the same TOA net radiation as the modal point, which is 80 W m^{-2} . The general shape of the histogram in Figure 2a is not unique to the tropical west Pacific region but is very similar in other convective regions of the tropics, such as in the Indian Ocean region.

Figure 2a also has a red line and a blue line superimposed on the histogram. The red line follows the maximum of the histogram at relatively low albedo, which falls in the region where the net radiation is greater than the modal value. The blue line follows the maximum of the histogram that occurs at relatively high albedo and low OLR. This line starts in the region of positive net radiation anomaly and runs across the black line to the region of net radiation that is less than the modal value.

Figure 2b shows the difference in net radiation at TOA for each point in the histogram, compared to the modal point. The heavy black line indicates 80 W m^{-2} net incoming radiation, which is both the average value and the value at the modal point. Blue indicates less and red indicates more net radiation than 80 W m^{-2} coming in at TOA. This heavy black line is the same one shown in Figures 2a and 2c.

Figure 2c shows the product of Figures 2a and 2b, divided by the total number of counts in the histogram. It shows that the clouds along the red line in Figure 2 make a substantial positive contrast from the net radiation of the modal point, but the cold bright clouds, which yield a TOA net radiation that is less than the modal value, offset this contribution. The sum over all the points in Figure 2c is -4 W m^{-2} , indicating the small difference between the largely clear modal scene and the average over all scenes.

Figure 2 shows that although the average net radiation is very close to the modal value of 80 W m^{-2} , the net radiation can vary greatly depending on the type and abundance of clouds present. Therefore, as Hartmann *et al.* [2001] pointed out, the similarity of the net radiation for relatively cloud free and average conditions cannot be a simple coincidence caused by the temperature of the tropopause and the optical depth of clouds with their tops near the tropopause, as Kiehl [1994] proposed, but requires a complex cancellation between clouds with relatively strong positive and negative effects on the radiation balance. The similarity of the net radiation for cloudy and clear conditions is a feature of the ensemble of clouds that is produced, and within that ensemble are clouds with both positive and negative cloud radiative effects that are more than an order

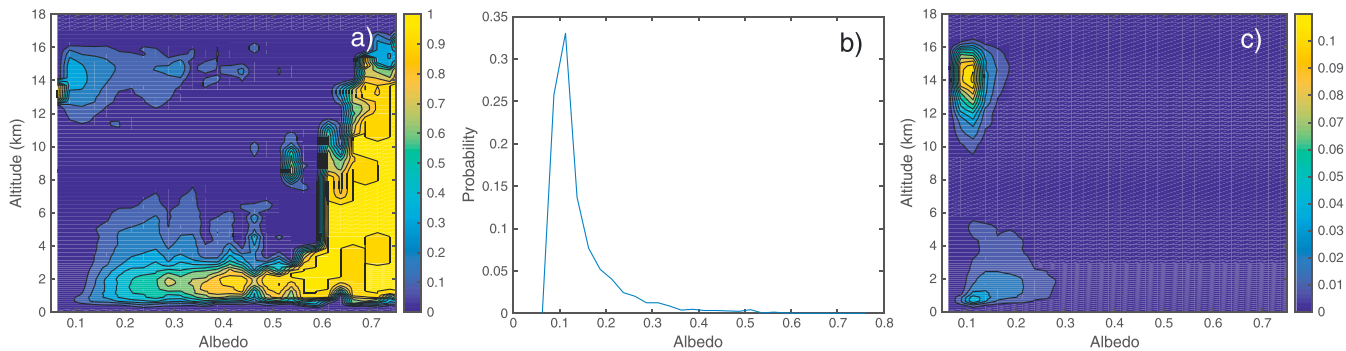


Figure 3. (a) CloudSat/CALIPSO cloud fraction as a function of altitude and CERES albedo for CERES OLR between 260 and 270 W m^{-2} , (b) probability of CERES albedo when CERES OLR is between 260 and 270 W m^{-2} , and (c) the product of Figures 3a and 3b.

of magnitude greater than their ensemble effect. The coldest and brightest clouds with an OLR of 100 W m^{-2} and an albedo of 70% yield a net TOA radiation that is about 75 W m^{-2} less than the average or modal net radiation. Clouds along the heavily occupied red line in Figure 2 can have net radiations that are greater than the modal value by a similar amount.

As the albedo increases and the OLR decreases from the modal value, two regimes can be discerned that are indicated with the red and blue lines in Figures 2a and 2c. The OLR decreases rather rapidly with increasing albedo along the red line, such that the net radiation increases with increasing albedo. For albedos greater than about 0.2, which is approximately the mean albedo for this region, and OLR of less than about 170 W m^{-2} , the histogram peaks along a line that corresponds to albedo increasing rather rapidly, while the OLR decreases less rapidly, indicating that the net radiation is decreased as the albedo increases. The cloud types indicated by the blue line are less common than those indicated by the red line. Clouds closest to the modal value, defined for OLR from 270 to 320 W m^{-2} and albedo from 0.05 to 0.2, constitute 38% of the scenes, while red line clouds, defined for OLR from 170 to 270 W m^{-2} and albedos from 0.05 to 0.25, constitute 32% of the scenes, while blue line clouds, defined for OLR from 90 to 180 and albedo from 0.3 to 0.8, constitute 17%.

2.2. Cloud Radiative Effects and Cloud Vertical Structure

The vertical structure of the clouds corresponding to the regimes indicated by the red and blue lines in Figure 2 can be investigated with the collocated cloud occurrence data from CloudSat-CALIPSO. To illustrate this, we make sections through Figure 2a that show the vertical structure of clouds for a particular OLR as a function of albedo. For an OLR bin of 10 W m^{-2} wide, the average fractional cloud occurrence is computed for albedo bins 0.025 wide and altitude ranges available from the CCCM data set (vertical spacing varies, but about 200 m). Figure 3 shows such a cross section for OLR values between 260 and 270 W m^{-2} or a central OLR of 265 W m^{-2} . From Figure 2 we see that this is a very frequently occurring range of OLR values, and that the albedo is most often around 7.5 to 10% for this range of OLR values.

Figure 3a shows the CloudSat-CALIPSO cloud fraction as a function of albedo averaged over all the scenes for which OLR falls in the range 260–270 W m^{-2} . It shows that an OLR near 265 W m^{-2} can be produced by high thin cloud or by midlevel and low cloud of various albedos. Figure 3b shows, however, that low albedos are much more common and the likely albedo for this OLR range peaks strongly near 0.1. Figure 3c shows the product of Figures 3a and 3b. This product gives the most likely vertical structure that you would see in this OLR range. It is a relatively thin cloud at an altitude of about 14 km with a planetary albedo around 0.1. Therefore, although tropical convective clouds are complex and varied, we can say that a region with an OLR of 265 W m^{-2} is most likely to have a thin cloud at 14 km, which is most likely the outflow from deep convection after it has thinned out a great deal, and possibly risen a little, although it is possible that some of this cloud is unrelated to convection. The effect of this type of cloud on the TOA radiation balance compared to the modal value is weakly positive. It increases the albedo by about 1%, so that if the incoming radiation is 410 W m^{-2} , it reduces the absorbed solar radiation by about 4 W m^{-2} . It reduces the emitted longwave radiation by about 289–265 = 24 W m^{-2} , so that the net radiative effect is about +20 W m^{-2} .

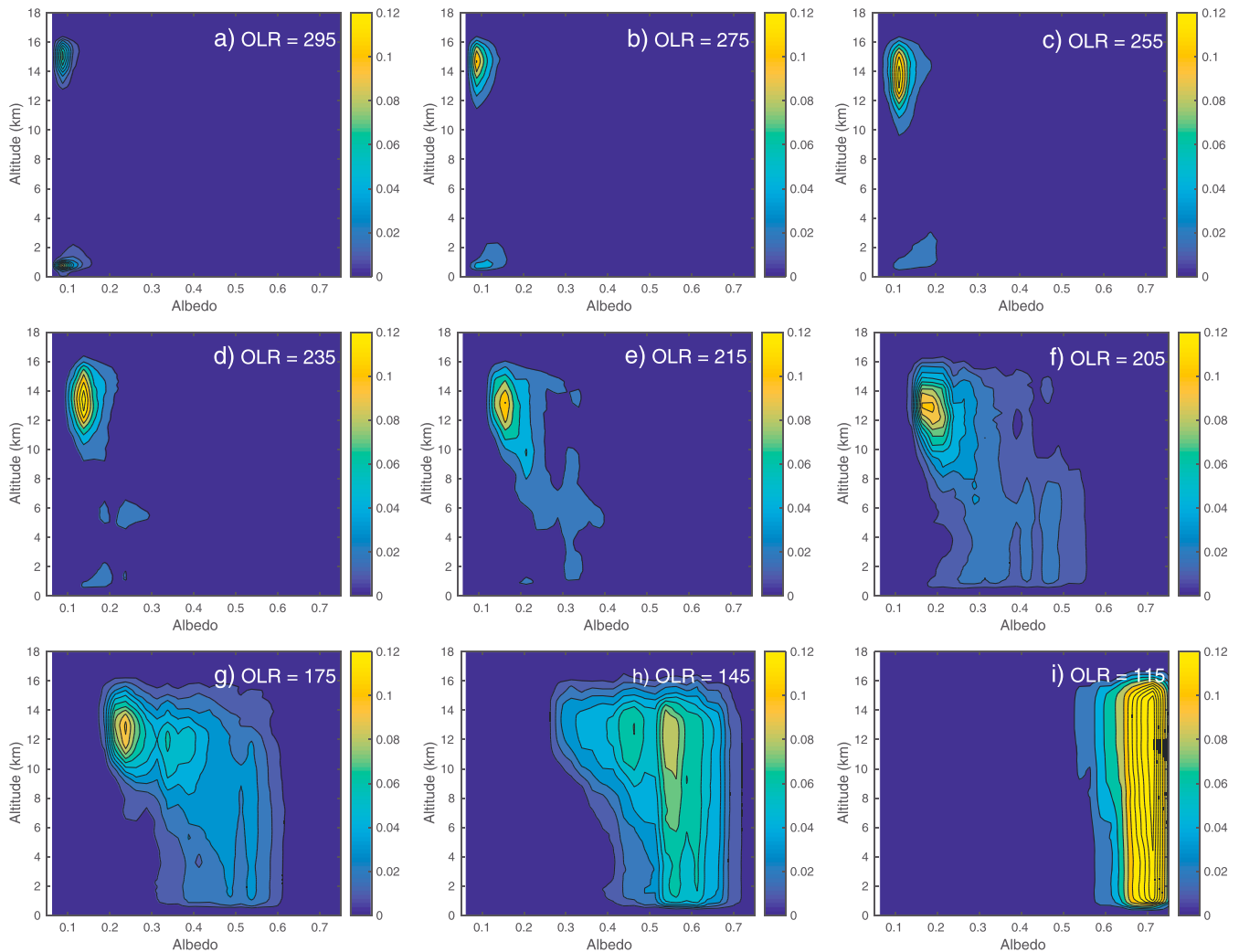


Figure 4. As in Figure 3c but for different ranges of OLR, centered on the values indicated in Figures 4a–4i.

To illustrate how the structure of the clouds changes with OLR, we repeat Figure 3c for different ranges of the OLR. In Figure 4a, for values of OLR centered on 295 W m^{-2} , we see that the scenes consist primarily of some infrequent thin cirrus centered near 15 km altitude, plus some boundary layer cloud. As we transition to lower values of OLR, the upper cirrus layer becomes more frequently occurring, moves downward to lower altitudes, and becomes physically thicker. For average OLR of 235 W m^{-2} , the cloud layer is centered at 13 km and extends from 10 to 16 km (Figure 4d). The central concentration at 13 km is at a temperature of about 215 K, which is consistent with the predictions of the Fixed Anvil Temperature Hypothesis [Hartmann and Larson, 2002; Kuang and Hartmann, 2007; Zelinka and Hartmann, 2010]. As the mean OLR is decreased further, the peak cloud occurrence remains at about 13 km and is confined between about the same altitudes, but becomes optically thicker, as is evidenced by the increasing albedo. For lower values of the OLR, such as 205 W m^{-2} , one begins to see evidence of midlevel clouds with tops near the freezing level at 6 km altitude, but these are less frequent than the anvil clouds centered on 13 km. For lower values of the OLR a transition is seen from mixed anvils and midlevel clouds at 205 W m^{-2} , to a mix of anvils and deep cells at 175 W m^{-2} , to pure rainy cores at 115 W m^{-2} and lower.

One can also composite these cloud occurrence histograms versus OLR for different values of the albedo (not shown). As one can guess from Figures 2a and 4, this gives a very similar story as that from the composites with respect to OLR in Figure 4. Low albedos correspond to thin anvil clouds and high OLR. As the albedo increases the anvil cloud gets thicker and the OLR decreases. For albedos greater than about 0.5 the cloud

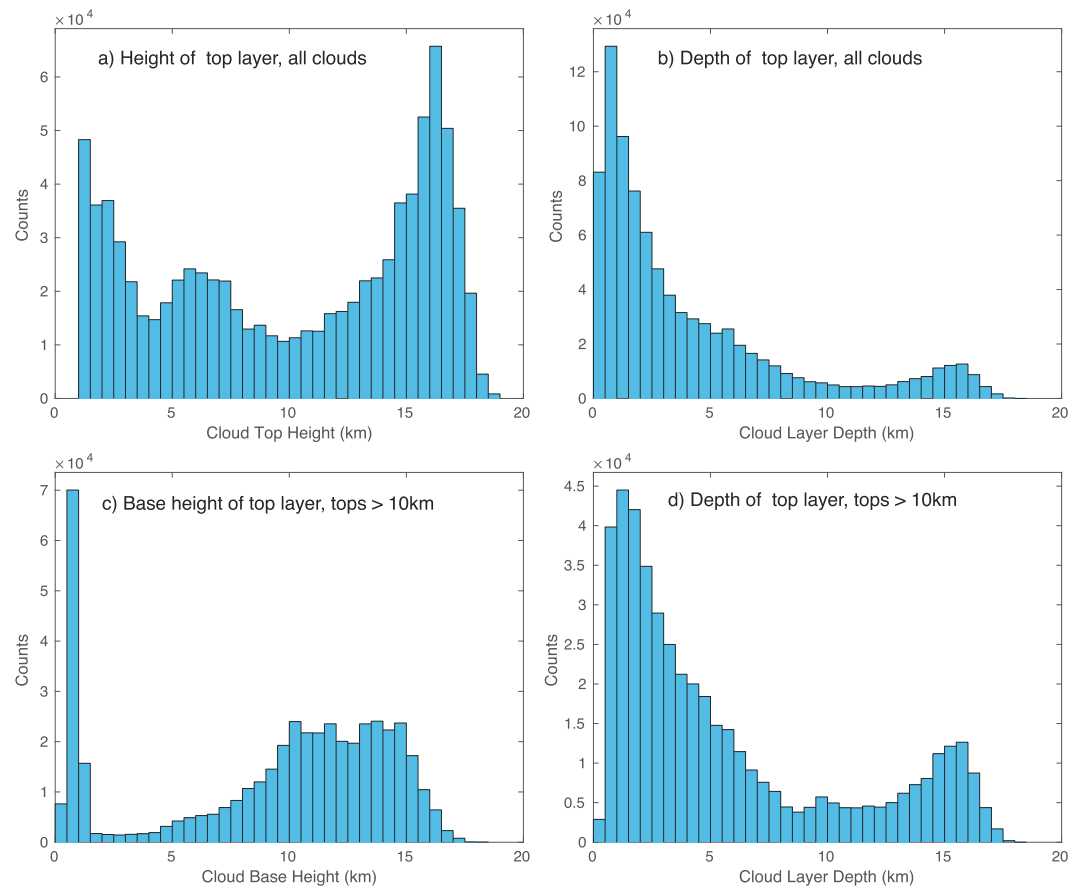


Figure 5. Histograms of (a) cloud top height and (b) cloud layer depth for clouds with tops between 1 and 20 km altitude, and (c) cloud base height and (d) cloud layer depth for clouds with tops between 10 and 20 km for the same region and dates as Figure 2.

increasingly extends to the surface, indicating the presence of rainy core clouds, and the OLR is about 150 W m^{-2} . As the albedo increases further, the cloud scenes are increasingly dominated by rainy cores that extend from a peak occurrence rate near 14 km to near the surface and the OLR continues to decrease.

From Figures 1–4 we infer that the net radiation in tropical convective regions is composed from cloud types whose net radiation can be $\pm 75 \text{ W m}^{-2}$ different from the modal or nearly clear-sky values, but that the ensemble of clouds adds up to a net radiation that is very similar to the modal value. From Figure 4 we conclude that upper tropospheric anvil clouds and the convective elements that support them dominate the cloud population. To first order, the population of clouds is a continuum from deep convective cores to thick anvils, to thin anvils to very thin clouds that were once anvils. The question of why the convective clouds produce little net radiation change from clear skies can thus be reduced to the question of the relative abundance of anvil clouds of various types. This can be further focused on the question of why thin anvil clouds are so abundant and thicker anvil clouds are less abundant, which is apparent from Figure 2. Also of interest is that the cloud tops stay at about the same altitude, rising a little for very thin clouds and for rainy cores. Most anvil clouds are characterized by a constant cloud top and a cloud base that becomes lower as the cloud becomes thicker and brighter, and the greatest concentration of anvil cloud frequency is around 13 km. In section 3 we will show that the major features in Figure 2a can be explained by anvil clouds that are centered near 13 km and vary in physical thickness and optical depth.

To provide a general view of the vertical structure of clouds in the region of interest, we consider the RL-GeoProf [Mace and Zhang, 2014] data of cloud height and thickness from the combined CloudSat-CALIPSO product. In Figure 5a we plot a histogram of the height of the top layer of clouds for the same region and time as Figure 2. This shows clearly the three modes of clouds in the convective tropics, with a top layer

of cirrus and anvil clouds, an intermediate congestus layer with tops at about the freezing level, and clouds in the boundary layer [Johnson *et al.*, 1999], as was also found in CloudSat data by Bacmeister and Stephens [2011]. The physical thickness, or depth, of these clouds is shown in Figure 5b. Here we see a peak occurrence of relatively thin clouds, with the occurrence decreasing rapidly for deeper clouds, and a small increase in frequency for clouds of depth 15–16 km, representing rainy cores for which radar returns extend from the boundary layer to near the tropopause. A relative minimum in cloud top occurrence occurs near 10 km. Since we are interested primarily in the anvil clouds with tops above 10 km, we show in Figures 5c and 5d the histogram of the base level and the depth for clouds with tops higher than 10 km. The cloud bases are mostly between 10 and 15 km, with the occurrence of bases decreasing rapidly below 10 km. It is very unlikely for a cloud with a top above 10 km to have a base between 8 km and 2 km. A maximum of cloud base occurrence appears between 500 and 1000 m, again indicating the rainy cores whose radar return extends from the boundary layer to above 10 km. For clouds with tops above 10 km, about 20% have bases below 2 km, indicating a substantial presence of convective cores and surrounding rainy areas.

3. Radiative Calculations

We consider an elevated layer cloud with varying physical and optical thickness. We use the RRTMG model to compute radiative fluxes for specified cloud optical properties [Clough *et al.*, 2005]. We use a vertical resolution of 500 m and long-lived greenhouse gas concentrations as observed. Surface albedo is set to 5%. We employ the parameterization for ice clouds from Fu [1996]. For effective particle radius and optical depth we take guidance from observations from van Diedenhoven *et al.* [2014], who indicate an effective radius of around 30 μm near tropical anvil tops, with increased particle sizes for lower cloud tops. We have experimented with various effective radii and with radii that increase lower in the cloud, but the conclusions from our calculations are not sensitive to these details and are well characterized by a constant effective radius of 30 μm . The mean thermal and moisture structure in the region of interest was obtained from ERA-Interim reanalysis data [Dee *et al.*, 2011] and is shown in Figure 6 averaged for the same region and times as Figure 2.

Houze [2014] states that anvil clouds have ice contents ranging from 0.001 to 0.5 g m^{-3} . Protat *et al.* [2010] show a distribution of ice water content for Darwin, Australia, that peaks near 0.01 g m^{-3} . For a 500 m thick layer this corresponds to ice water path of 5 g m^{-2} . We will consider two progressions of anvil cloud shape: (1) an anvil with a fixed depth and triangular distribution of ice content for which the peak content is increased in small increments, and (2) an anvil with a fixed central altitude that thickens both in physical depth and in ice content (Figure 7). The second example intends to mimic how tropical anvil clouds form, spread, and dissipate. We imagine that they start out as thick anvil outflows from deep convection, and that these anvil clouds spread, thin out, and eventually dissipate. We model this in reverse by considering a cloud with a top at the outflow level of 12.25 km that is 500 m thick and has a low ice water content of 0.014 g m^{-3} , for a total ice water path of 7 g m^{-2} . We then simultaneously increase both the thickness and the ice water content of the cloud, as indicated in Figure 7b.

Figure 8 shows the effect on the TOA radiation balance of the thickening of the anvil clouds specified in Figure 7. The OLR at first decreases rapidly but then remains relatively constant once the ice path exceeds about 50 g m^{-2} . The albedo increases steadily with ice path but more slowly as the cloud becomes optically thicker. The net radiation at first increases and then decreases as the ice path exceeds about 50 g m^{-2} . A thick cloud with a high ice content strongly reduces the net radiation balance at the top of the atmosphere and the surface, consistent with Figures 1–4. The cloud also reduces the OLR significantly, but the OLR for cloud with high ice content is sensitive to the altitude of the cloud top but not sensitive to the cloud base altitude. For both specifications of cloud, the net radiation first increases, because of the longwave effect, but then decreases because the albedo increases as the cloud thickens, even after the OLR becomes insensitive to the cloud thickness. Net radiation is insensitive to ice path near 50 g m^{-2} .

The presence of the cloud also has a strong effect on the heating rate within the atmosphere. Figure 9 shows the atmospheric heating rate for the clouds specified in Figure 7, along with the clear-sky heating rate. Figure 9a shows that when the cloud is very thin, the cloud layer is heated and the cooling rate of the clear air below the cloud is reduced. As the cloud becomes thicker, very strong heating and cooling rates develop near the bottom and top of the cloud, respectively. Since this heating-cooling dipole is primarily driven by

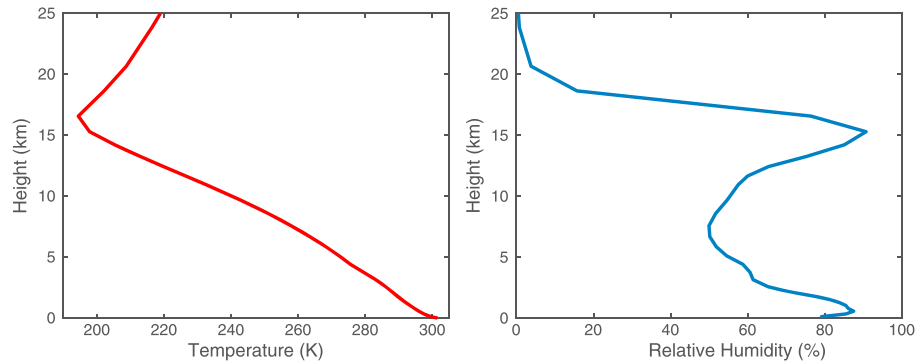


Figure 6. Temperature and relative humidity profiles from ERA Interim for the western equatorial Pacific in July and August.

longwave radiation, it saturates and becomes less sensitive to variations in ice content for thicker clouds. This behavior is also seen in Figure 9b, where the cooling rates follow the edge of the cloud but do not change much in magnitude as the ice content of the cloud is increased. Below the cloud, the clear-sky heating rate of about 1.75 K d^{-1} at 10 km is reduced to near zero for moderately thick anvils. This can have a significant impact by removing the radiative destabilization of the troposphere beneath the cloud, as well as by warming the atmosphere.

The very strong heating and cooling rates near the top and bottom of anvil cloud layers cannot be sustained for very long and must evoke a response in mean vertical motion, in vertical mixing within the cloud, or in cloud evaporation. Vertical motion will likely thin the cloud by spreading it [Dinh et al., 2010; Durran et al., 2009; Lilly, 1988]. Mixing at the top will mix in warm, dry air, and mixing at the bottom will mix in lower energy air. Both of these mixing processes will also act to thin the cloud. So the atmospheric cloud radiative effect in the cloud layer will drive processes that tend to thin the cloud, especially clouds that have relatively high ice concentrations and sharp gradients in the vertical. Higher ice concentrations will also experience increased ice removal due to aggregation and sedimentation. On the other hand, heating below and cooling above may drive convection that sustains the cloud.

In the net, the layer in which the cloud resides is heated by radiation, especially when the cloud base is high. The bottom of the cloud traps the emission from below and emits downward at a lower temperature than the upward emission temperature of the underlying atmosphere. Figure 10 shows the heating rate averaged over the mass of the cloud layer, which is integrated between the pressure of cloud top p_{ct} and cloud base p_{cb} . (1).

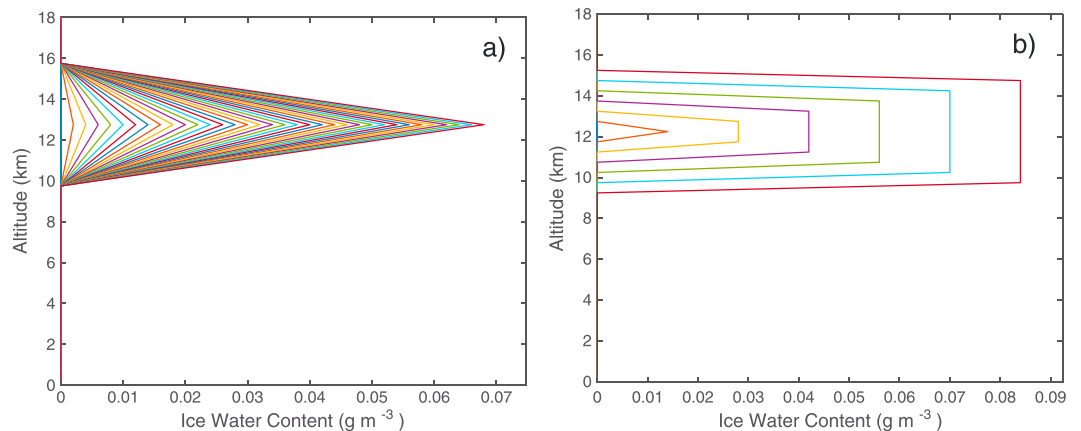


Figure 7. Ice water content as a function of altitude for cases representing (a) increasing ice content of triangular cloud and (b) simultaneous physical thickening and ice content increase of anvil cloud.

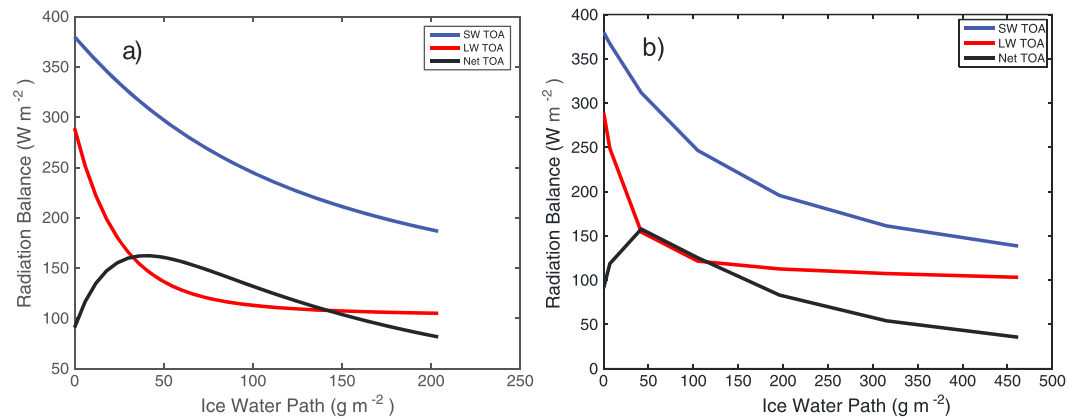


Figure 8. Absorbed solar, OLR, and Net Radiation at TOA as functions of ice water path for the two anvil progressions in Figure 7, plotted as a function of the total ice path. In each case the clear-sky value is plotted at zero ice water path.

$$\frac{\partial T \int_{p_{ct}}^{p_{cb}} \frac{\partial T}{\partial t} dp}{\partial t \int_{p_{ct}}^{p_{cb}} dp} \tag{1}$$

For the cloud with fixed base and top heights, the heating rate at first increases and then levels off as the ice content is increased. For the cloud that grows both in depth and ice concentration, the heating rate first

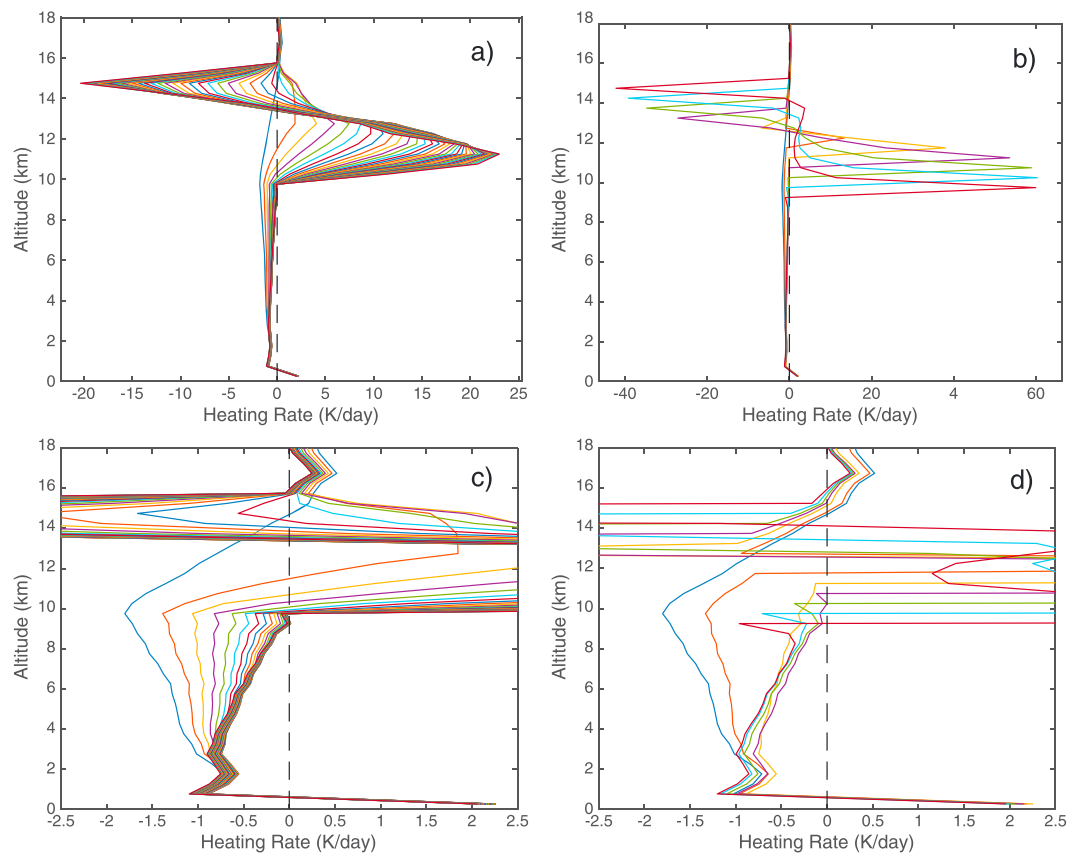


Figure 9. Atmospheric heating rate in degrees per day for the anvil clouds in Figure 7. Color code is the same as Figure 7. Figures 9c and 9d show an expanded heating rate scale to reveal the heating rate changes in the clear layer below the anvil cloud.

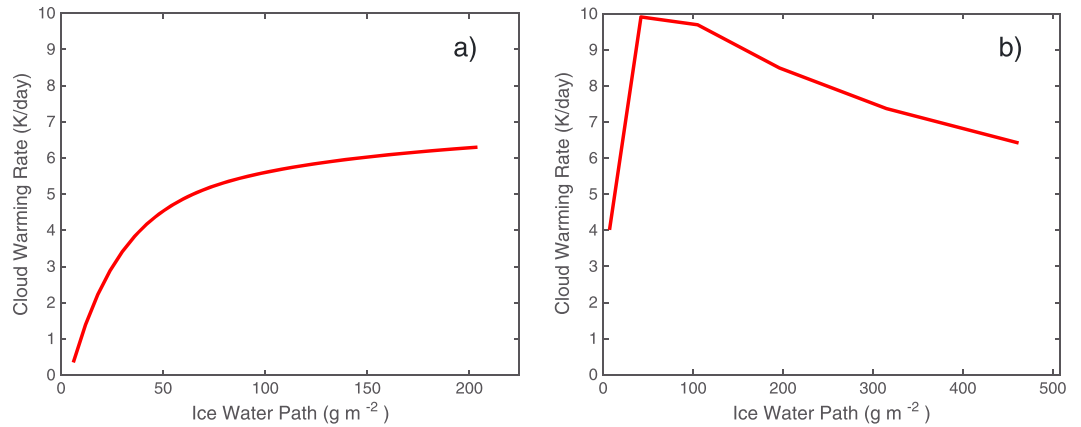


Figure 10. Heating rate integrated across the mass of the cloudy layer for the same cases as in Figure 7.

increases, then decreases as the cloud becomes thicker. This is because as the bottom of the cloud gets lower, the net upward longwave flux at the cloud base decreases, since the cloud base is getting warmer and emitting more strongly downward. If the cloud top is fixed in altitude, and the cloud base is lowered while maintaining the same ice concentration in each layer, the net heating rate of the cloud layer decreases to near zero as the bottom of the cloud approaches the boundary layer (results not shown here, but see *Ackerman et al. [1988]*). For a very thick cloud extending from near the surface to near the tropopause, the net radiative heating rate is very small, since the net heating at the base is similar to the emission at cloud top and the mass of the cloud layer is large. Optically thick clouds with bases at high altitude are very strongly heated by both longwave and shortwave radiation and must either evaporate or rise rapidly. Clouds with intermediate optical depths and intermediate thicknesses have modest but positive, mass-average heating rates combined with a strong dipole heating at the bottom and cooling at the top of the cloud. It is thus the intermediate optical depth clouds with elevated cloud bases that are favored by radiative heating, which tends to destabilize the cloud layer. If the cloud is being sustained by radiative heating, then the integrated cloud radiative heating peaks for clouds with a preferred depth, and we might expect clouds of this intermediate thickness to be more abundant, if a steady response to radiative heating is a good model for anvil clouds. Of course, the supply of condensed water from the convective cores and the response of the microphysics to increasing ice concentrations are critically important.

Figure 11 shows the albedo-OLR pairings for the clouds in Figure 7 in the same coordinate system as Figure 2. We see that the thickening anvil cloud progression can reproduce the clustering of occurrences along the red and the blue lines in Figure 2. Thin anvil clouds produce the cluster of points along the red line in Figure 2,

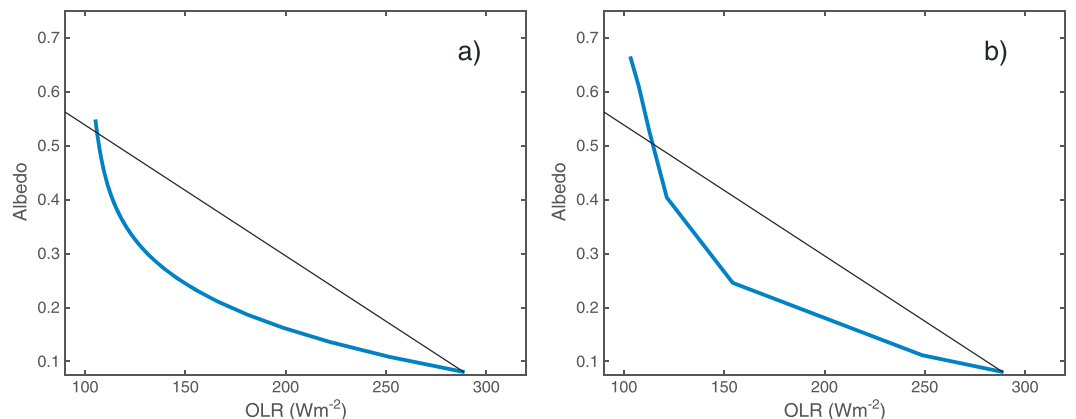


Figure 11. Albedo versus OLR plots for the two sets of cases shown in Figure 7. Black line is the same as the black line in Figure 2. Clear-sky values are also plotted.

and as these thicken further they produce the more steeply sloped blue line, which represents convective cores and surrounding rainy areas. We thus conclude that the effect of clouds on the radiation balance in the convective tropics can be characterized by anvil clouds of varying thickness, with the very thickest clouds with the coldest tops representing the rainy cores. From this perspective, the explanation for the net radiation neutrality of tropical convective clouds in the warm pool area rests upon understanding how the occurrence frequency of anvil clouds of various optical thicknesses is determined.

It is reasonable to suppose that a certain number of high optically thick clouds must exist to produce the rainfall in the tropics, and the question then becomes how much anvil cloud is produced and how the optical depth of that anvil cloud is determined. Clearly, anvil cloud spreads from convection and thins as it does so, and this would predict that the area coverage of anvil cloud should exceed that of convective cores, but what processes control total area and the mean and variance of the optical depth of those detrained anvil clouds? It is also clearly important to understand how this distribution of anvil clouds might change in a warmed Earth and whether the current generation of climate models is capable of simulating the key processes. These questions should be given a high priority in climate research.

4. Heating Rates Computed From Cloud Observations

In this section we present an analysis of the heating rates computed from the CloudSat-CALIPSO data, as described in *L'Ecuyer et al.* [2008] and *Henderson et al.* [2013], and available as the 2B_FLXHR-LIDAR data set from the CloudSat Data Processing Center. A radiative transfer model is used to calculate fluxes and heating rates at each cloud profiling radar range gate from the surface to the lower stratosphere. Broadband fluxes and heating rates are consistent with the liquid and ice water content estimates from CloudSat, CALIPSO, and MODIS. We organize the data by choosing scenes in which anvil cloud with a top and bottom occur at the same levels as in Figure 7b. The cloud structure was searched to find observations in the region of interest for which the top and bottom of a high cloud layer are within 500 m of the values given for Figure 7b, and for which no cloud is observed between the cloud base and 3 km altitude. A large sample of such cases was then averaged together to give the mean profiles shown in Figure 12. The standard deviation is about twice the mean values shown in these plots. The mean heating rates are smaller than in the calculations shown in Figure 7, but the general shapes are consistent and the magnitude of the heating rates are still significant. We did not control for the ice content, which is simply whatever was observed for the cases we selected, so consistent relationship between cloud physical thickness and cloud optical thickness that we prescribed in Figure 7b is not necessarily represented by the observations. Nonetheless, the magnitude of the heating rates tends to increase with the physical thickness of the cloud.

5. Single Column Model Experiments

To quantitatively demonstrate how tropical anvil effects on atmospheric radiative heating influence their top-of-atmosphere cloud radiative effect (CRE) would be a long undertaking requiring considerable model development and validation, but it is a good long-term science goal. This will involve properly considering the effects of large-scale and mesoscale motions and the dependence on cloud microphysical parameterizations. Here we use a much simpler approach to try to generate interest in this idea. Using the single column model of the CAM5, SCAM5 (CESM v1.2.2), we can easily demonstrate that cloud radiative effect on atmospheric heating rates change the ice water content and its variability significantly. The increased variability indicates strong feedbacks between the amount of anvil ice and its generation by physical processes in the atmosphere. Also, it will be apparent that not only the radiative effect on the cloud layer but also the effects on the heating rate below the anvil cloud are important. Future work can explore these questions with eddy resolving models of the anvil cloud and models with enough spatial extent to properly account for the effects of mesoscale motions.

As a test case we use the forcing for the Tropical Ocean Global Atmosphere Experiment 2 (TOGAII) intensive observing period, which is provided as a standard test case with the SCAM5 software. This version uses a modified *Zhang and McFarlane* [1995] convection scheme, the moist turbulence scheme of *Bretherton and Park* [2009] and the shallow convection scheme of *Park and Bretherton* [2009], the ice microphysics of *Morrison and Gettelman* [2008] [*Gettelman et al.*, 2010], and the RRTMG radiation scheme [*Iacono et al.*, 2008; *Mlawer et al.*, 1997]. The SCAM5 is forced with the large-scale vertical velocity and heat and moisture

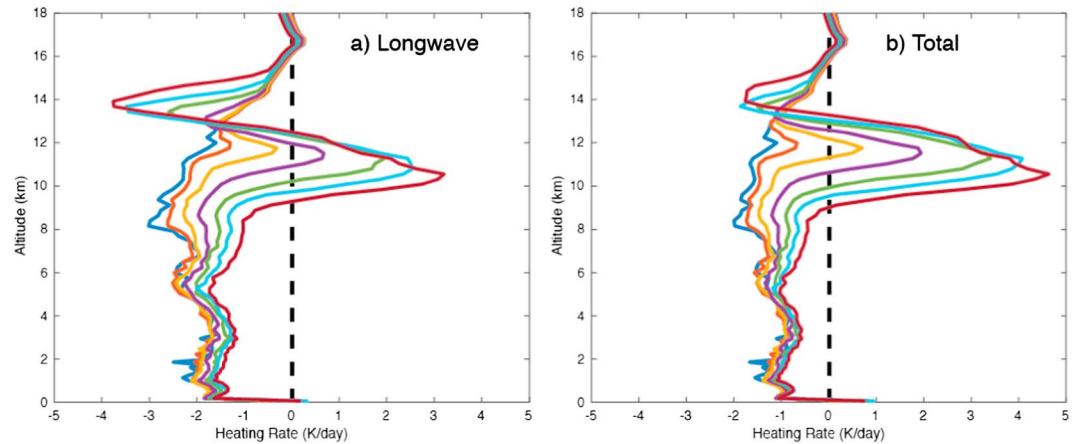


Figure 12. Average (a) longwave and (b) total heating rates computed from observations for cloud layers with the same top and bottom altitudes as in Figure 7b. The color code is the same as in Figure 7b.

fluxes computed from reanalysis for the TOGAII intensive observing period (IOP). To simplify things further, we average the large-scale forcing over the 21 day TOGAII IOP period and extend this average forcing over 42 days to provide steady forcing over a longer period. The only modification to the averaged TOGA II IOP forcing that is applied is a small moisture source of $2 \times 10^{-9} \text{ kg kg}^{-1} \text{ s}^{-1}$ at all levels from 165 hPa to 965 hPa. This is to counteract a slight drying tendency of the SCAM5 that would otherwise lead to a steady cooling of the atmosphere over the period, even though the surface temperature is fixed. With this modification the trend of temperature over the integration period is small. The moisture source also gives a more persistent and thicker anvil cloud.

To test the importance of the anvil cloud effects on the atmospheric radiative heating rate, we run a separate case in which the model feels the clear-sky radiative heating rates instead of the full radiative effect including the clouds. The same large-scale forcing is applied in both cases. Figure 13 shows the ice water path as a function of time and the average ice water content as a function of height for the cases with and without the cloud radiative effects included. The ice water path is approximately doubled, is much more variable, and is shifted upward in the atmosphere when the cloud radiative effects are included.

Figure 14 shows the radiative heating rates for average and for clear-sky conditions and their difference, which is the heating rate effect of clouds. The clear-sky heating rate is similar in the two cases, but the radiative effect of clouds is to reduce the cooling rate below the anvil cloud and increase it in the upper half of the anvil layer. Since the anvil cloud is thicker and higher in the case where cloud radiative effects are included, the heating below the anvil is stronger and the cloud top cooling occurs at a greater altitude. These changes

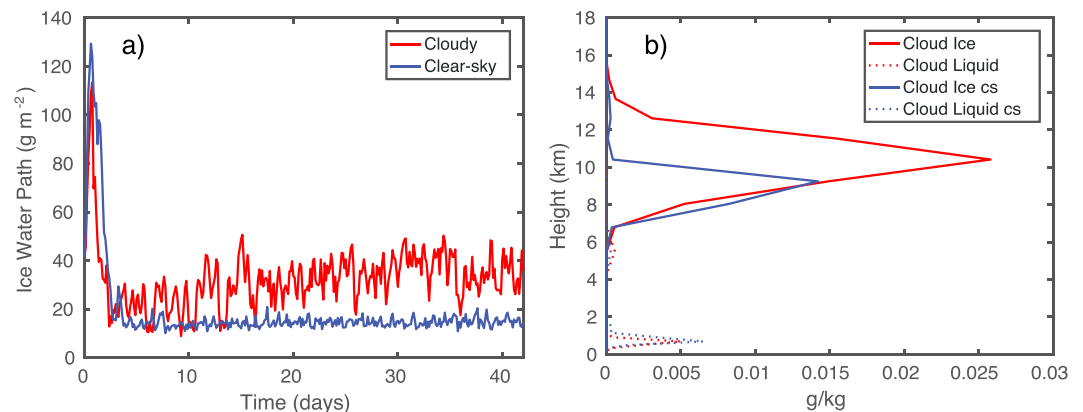


Figure 13. (a) Ice water path every 3 h for TOGAII SCAM5 cases with cloudy-sky and clear-sky radiation as a function of time, and (b) time average ice and liquid mixing ratios as functions of altitude for the same two cases.

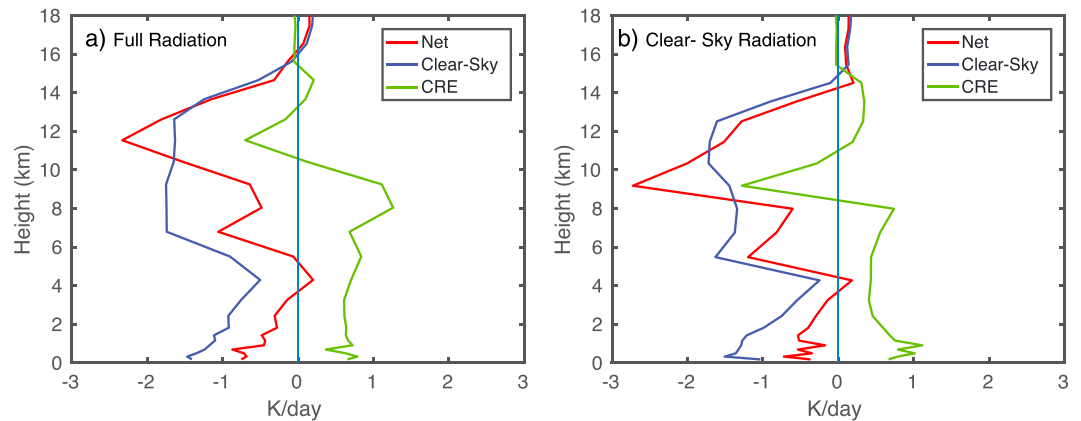


Figure 14. Net, clear-sky, and cloud radiative effect (CRE) on radiative heating rate for the TOGAll case (a) with full radiative interactions and the case (b) in which the clear-sky radiative heating rate is applied. Note that the net heating rate and CRE are shown for the run in which the clear-sky cooling was applied, but the model did not feel the radiative effects of the clouds in this case.

in cloud effects help to sustain the anvil cloud locally, but the precipitation is reduced somewhat because the overall atmospheric radiative cooling is reduced, which also results in a net warming of the temperature profile (Table 1). So when cloud radiative effects are included, a thicker and higher anvil cloud is produced with a reduced precipitation rate. Less precipitation falls from convection, but ice reaches a higher altitude and is sustained longer when cloud radiative effects are included.

Some of the key heating rate terms are shown in Figure 15. The prescribed large-scale upward motion extends to above 16 km. At the top of this layer is a region where the heating associated with the deep convection scheme does not penetrate. This layer has a lapse rate that is very near the dry adiabatic lapse rate, and cooling by downward mixing of potential temperature by the turbulence scheme is balanced by warming by moist processes, since the large-scale upward motion advects moisture into this layer. The production of ice cloud by moist processes in this adiabatic layer is small compared to the production of ice by detrainment from the deep convection scheme, and the radiative effects of this ice are also smaller. In the case without the radiative effects of clouds, this layer is much deeper and the turbulence is stronger. The turbulence appears to be driven by the lapse rate tendency associated with the rapid reduction of the deep convective heating with altitude that occurs below the dry adiabatic layer. Without cloud radiative effects this cutoff in heating associated with the deep convection scheme is sharper and occurs lower in the atmosphere. The radiative heating rate with cloud radiative effects included has stronger cooling near 12 km and weaker cooling below the cloud compared to the case in which cloud radiative effects are excluded. The warming below is important in raising the top of the layer in which deep convection dominates. The cloud radiative heating thus interacts with the various parameterizations in the single column model to produce a quite different equilibrium temperature profile and ice cloud amount. Whether these simulations are in any way reflective of reality is an open question, but it is clear that the radiative effects of anvil clouds can have a strong effect of the amount of ice cloud produced in this system.

Although the atmosphere is made warmer and moister by the radiative effects of anvil clouds, which results in an increase in anvil cloud, the overall cooling rate of the atmosphere and the associated rainfall rate are

Table 1. Comparison of Some Quantities for the TOGAll SCAM5 Simulations With and Without Cloud Radiative Effects^a

	Full Radiation Case	Clear-Sky Radiation Case
Precipitation (mm d^{-1})	9.6 (9.8)	10.6 (10.6)
SWCRE (W m^{-2})	-101.7 (-89.3)	-71.2 (-79.7)
LWCRE (W m^{-2})	74.0 (61.4)	51.1 (61.4)
NetCRE (W m^{-2})	-27.8 (-27.9)	-20.1 (-18.3)
Temperature (K)	259.9 (259.5)	257.8 (257.6)

^aMean temperature is averaged across all layers in the troposphere. Numbers in parenthesis are for the case in which the large-scale vertical velocity was varied sinusoidally from zero to twice its mean value with a 4 day period.

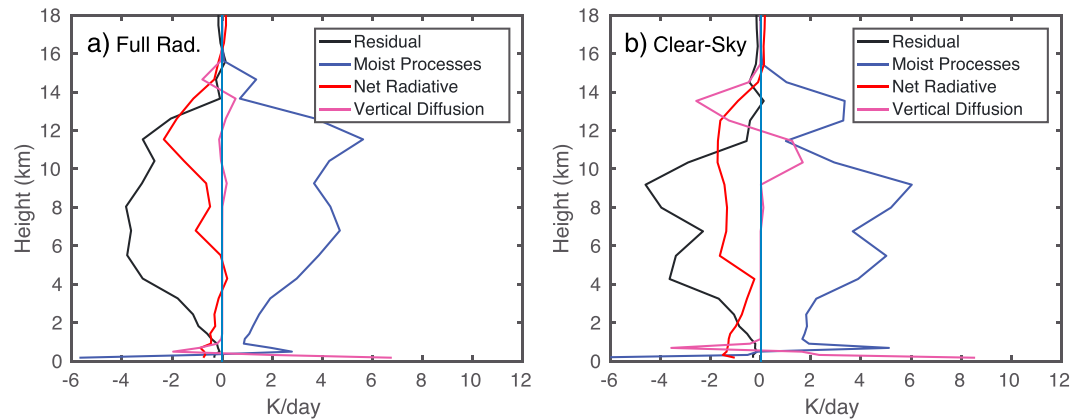


Figure 15. Contributions of various terms to the heating rate from the TOGALL integrations for the (a) full radiation and (b) clear-sky radiation cases.

reduced by the atmospheric cloud radiative effects, giving the possibility of a negative feedback between anvil cloud amount and the supply of ice by deep convection. The amount of ice in the anvil is, however, dependent on the large-scale vertical motion field and the microphysical processes that remove ice by sedimentation and other processes. The current set of experiments has no feedback on mean vertical motion by cloud properties, since the large-scale vertical motion is fixed.

We have done a number of alternative cases to test the robustness of these results. The radiative effect of the clouds is always important, but the magnitude of the difference is dependent on the amount of ice cloud present in the control case. Also, if we simulate synoptic variability by oscillating the large-scale vertical velocity forcing around its mean value with a period of 4 days and an amplitude equal to its mean value, the response of ice cloud amount to cloud radiative effects is much less, but the column is warmed by the radiative effect of the ice cloud by a similar amount and this raises the ice cloud altitude. The cloud radiative effects also reduce the precipitation by a similar amount in this case (Table 1). The enhancement of SWCRE by cloud radiative effects is reduced from -30 W m^{-2} in the steady case to -10 W m^{-2} in the case with oscillating vertical velocity. The ice cloud disappears when the vertical motion is small or downward and is less sensitive to radiation when the motion is strongly upward.

6. Conclusion

A combination of top-of-atmosphere radiation budget measurements from CERES and vertical cloud structure data from CLOUDSAT-CALIPSO has been used to study the relationship of the vertical structure of tropical convective clouds to the TOA radiation budget anomalies they produce in that part of the West Pacific Warm Pool where longwave and shortwave cloud radiative effects approximately cancel. The cancellation results from the particular frequency of thin versus thick anvil clouds that occurs there. Using a radiative transfer model, it was shown that the shape of the histogram of cloud occurrence as a function of albedo and OLR can be explained as variations in the physical and optical thickness of an elevated anvil cloud layer. To explain the net radiative effect of the cloud population, one must explain how the frequency of occurrence of thick versus thin anvil clouds is determined.

One important factor in determining the frequency of occurrence of anvil clouds of varying thickness is the effect of radiation on those anvils. Radiation generally encourages the persistence of moderately thick anvils by heating their bottoms and cooling their tops, and thereby encouraging convection within the anvil clouds. Heating the entire cloud layer also helps the clouds to persist, if the cloud layer is then lifted rather than increasing its temperature. As anvil clouds become physically thicker, and their cloud base is lowered, the downward emission from their cloud bases increases and the net radiative heating of the cloud layer is decreased. Convective cores are thus not encouraged by direct radiative heating, whereas elevated clouds of moderate thickness are encouraged to persist both by heating, which would tend to lift the cloud relative to nearby clear skies, and also by destabilizing the cloud layer by heating at the bottom and cooling at the

top. Anvil clouds also make deep convection deeper by warming the lower troposphere and cooling near the top of the convecting layer.

Experiments with a single-column model are performed to show that the radiative effects of anvil clouds have a large impact on the character of the anvil clouds even in the presence of large-scale forcing. For the time-averaged large-scale forcing of the TOGA intensive observing period, the radiative effects of the anvil clouds cause the anvils to be higher and thicker and to show much more variability than when cloud radiative effects are excluded from the simulation. This occurs because the anvil clouds produce warming below the anvil and cooling in the anvil layer. The warming below suppresses the intensity of deep convection, but the cooling in the anvil layer encourages anvil ice and deepens the convection. The competition between these two effects, combined with cloud physical processes that remove ice, could lead to cirrus optical depths of intermediate values, which help produce longwave and shortwave effects that nearly balance across the ensemble of anvil clouds.

Tropical convective clouds in climate models are highly parameterized, and global models cannot resolve the small-scale circulations in convective cloud systems that are likely important in determining their optical properties and area coverage. The hypothesis that radiative heating drives tropical anvil clouds toward a particular distribution of anvil cloud optical thickness that favors a near neutral radiation balance might be advanced with a set of experiments with a cloud-resolving model that has very realistic microphysics and radiative transfer, and also sufficient spatial resolution to resolve the convective structures within anvil clouds that may develop in response to radiative heating and help to sustain the anvils. Experiments by *Fu et al.* [1995] and *Harrop and Hartmann* [2016] suggest that radiative heating of the cloud modifies anvil cloud structure, but a realistic simulation of the observed histogram of albedo and OLR pairings in Figure 2a has probably yet to be accomplished.

Acknowledgments

We thank C.S. Bretherton for helpful discussions and Marc L. Michelsen for computer assistance. The CAM5 model code was downloaded from the National Center for Atmospheric Research. Satellite data were obtained from the NASA Langley Atmospheric Sciences Data Center (https://eosweb.larc.nasa.gov/HORDERBIN/HTML_Start.cgi) and the CloudSat Data Processing Center (<http://www.cloudsat.cira.colostate.edu/>). This work was supported by NASA grant NNX14AJ26G to the University of Washington.

References

- Ackerman, T. P., N.-L. Kuo, F. P. J. Valero, and L. Pfister (1988), Heating rates in tropical anvils, *J. Atmos. Sci.*, *45*(10), 1606–1623, doi:10.1175/1520-0469(1988)045<1606:HRITA>2.0.CO;2.
- Bacmeister, J. T., and G. L. Stephens (2011), Spatial statistics of likely convective clouds in CloudSat data, *J. Geophys. Res.*, *116*, D04104, doi:10.1029/2010JD014444.
- Berry, E., and G. G. Mace (2014), Cloud properties and radiative effects of the Asian summer monsoon derived from A-Train data, *J. Geophys. Res. Atmos.*, *119*, 9492–9508, doi:10.1002/2014JD021458.
- Bretherton, C. S., and S. Park (2009), A new moist turbulence parameterization in the community Atmosphere model, *J. Clim.*, *22*(12), 3422–3448, doi:10.1175/2008jcli2556.1.
- Clough, S. A., M. W. Shephard, E. Mlawer, J. S. Delamere, M. Iacono, K. Cady-Pereira, S. Boukabara, and P. D. Brown (2005), Atmospheric radiative transfer modeling: A summary of the AER codes, *J. Quant. Spectrosc. Radiat. Transfer*, *91*(2), 233–244, doi:10.1016/j.jqsrt.2004.05.058.
- Dee, D. P., et al. (2011), The ERA-Interim reanalysis: Configuration and performance of the data assimilation system, *Q. J. R. Meteorol. Soc.*, *137*(656), 553–597, doi:10.1002/qj.828.
- Deng, M., G. G. Mace, and Z. Wang (2016), Anvil productivities of tropical deep convective clusters and their regional differences, *J. Atmos. Sci.*, *73*, 3467–3487, doi:10.1175/JAS-D-15-0239.1.
- Dinh, T. P., D. R. Durran, and T. P. Ackerman (2010), Maintenance of tropical tropopause layer cirrus, *J. Geophys. Res.*, *115*, D02104, doi:10.1029/2009JD012735.
- Durran, D. R., T. Dinh, M. Ammerman, and T. Ackerman (2009), The mesoscale dynamics of thin tropical tropopause cirrus, *J. Atmos. Sci.*, *66*(9), 2859–2873, doi:10.1175/2009jas3046.1.
- Fu, Q. (1996), An accurate parameterization of the solar radiative properties of cirrus clouds for climate models, *J. Clim.*, *9*(9), 2058–2082.
- Fu, Q., S. K. Krueger, and K. N. Liou (1995), Interactions of radiation and convection in simulated tropical cloud clusters, *J. Atmos. Sci.*, *52*(9), 1310–1328.
- Gottelman, A., X. Liu, S. J. Ghan, H. Morrison, S. Park, A. J. Conley, S. A. Klein, J. Boyle, D. L. Mitchell, and J. L. F. Li (2010), Global simulations of ice nucleation and ice supersaturation with an improved cloud scheme in the Community Atmosphere Model, *J. Geophys. Res.*, *115*, D18216, doi:10.1029/2009JD013797.
- Harrison, E. F., P. Minnis, B. R. Barkstrom, V. Ramanathan, R. D. Cess, and G. G. Gibson (1990), Seasonal variation of cloud radiative forcing derived from the Earth radiation budget experiment, *J. Geophys. Res.*, *95*, 18,687–18,703, doi:10.1029/JD095iD11p18687.
- Harrop, B. E., and D. L. Hartmann (2016), The role of cloud heating within the atmosphere on the high cloud amount and top-of-atmosphere cloud radiative effect, *J. Adv. Model. Earth Syst.*, *8*, 1391–1410, doi:10.1002/2016MS000670.
- Hartmann, D. L., and D. A. Short (1980), On the use of earth radiation budget statistics for studies of clouds and climate, *J. Atmos. Sci.*, *37*(6), 1233–1250.
- Hartmann, D. L., and K. Larson (2002), An important constraint on tropical cloud-climate feedback, *Geophys. Res. Lett.*, *29*(20), 1951–1954, doi:10.1029/2002GL015835.
- Hartmann, D. L., L. A. Moy, and Q. Fu (2001), Tropical convection and the energy balance at the top of the atmosphere, *J. Clim.*, *14*(24), 4495–4511, doi:10.1175/1520-0442(2001)014<4495:TCATEB>2.0.CO;2.
- Henderson, D. S., T. L'Ecuyer, G. Stephens, P. Partain, and M. Sekiguchi (2013), A multisensor perspective on the radiative impacts of clouds and aerosols, *J. Appl. Meteorol. Climatol.*, *52*(4), 853–871, doi:10.1175/jamc-d-12-025.1.
- Houze, R. A. (1982), Cloud clusters and large-scale vertical motions in the tropics, *J. Meteorol. Soc. Jpn.*, *60*, 396–410.

- Houze, R. A. (2014) *Cloud Dynamics*, pp. 130–131, Elsevier, Amsterdam.
- Iacono, M. J., J. S. Delamere, E. J. Mlawer, M. W. Shephard, S. A. Clough, and W. D. Collins (2008), Radiative forcing by long-lived greenhouse gases: Calculations with the AER radiative transfer models, *J. Geophys. Res.*, *113*, D13103, doi:10.1029/2008JD009944.
- Igel, M. R., A. J. Drager, and S. C. van den Heever (2014), A CloudSat cloud object partitioning technique and assessment and integration of deep convective anvil sensitivities to sea surface temperature, *J. Geophys. Res. Atmos.*, *119*, 10,515–10,535, doi:10.1002/2014JD021717.
- Johnson, R. H., T. M. Rickenbach, S. A. Rutledge, P. E. Ciesielski, and W. H. Schubert (1999), Trimodal characteristics of tropical convection, *J. Clim.*, *12*(8), 2397–2418.
- Kiehl, J. T. (1994), On the observed near cancellation between longwave and shortwave cloud forcing in tropical regions, *J. Clim.*, *7*(4), 559–565.
- Kuang, Z., and D. L. Hartmann (2007), Testing the fixed anvil temperature hypothesis in a cloud-resolving model, *J. Clim.*, *20*, 2051–2057, doi:10.1175/JCLI4124.1171.
- Kubar, T. L., D. L. Hartmann, and R. Wood (2007), Radiative and convective driving of tropical high clouds, *J. Clim.*, *20*(22), 5510–5526, doi:10.1175/2007jcli1628.1.
- L'Ecuyer, T. S., N. B. Wood, T. Haladay, G. L. Stephens, and P. W. Stackhouse (2008), Impact of clouds on atmospheric heating based on the R04 CloudSat fluxes and heating rates data set, *J. Geophys. Res.*, *113*, D00A15, doi:10.1029/2008JD009951.
- Lilly, D. K. (1988), Cirrus outflow dynamics, *J. Atmos. Sci.*, *45*(10), 1594–1605.
- Mace, G. G., and Q. Q. Zhang (2014), The CloudSat radar-lidar geometrical profile product (RL-GeoProf): Updates, improvements, and selected results, *J. Geophys. Res. Atmos.*, *119*, 9441–9462, doi:10.1002/2013JD021374.
- Mace, G. G., Q. Q. Zhang, M. Vaughan, R. Marchand, G. Stephens, C. Trepte, and D. Winker (2009), A description of hydrometeor layer occurrence statistics derived from the first year of merged Cloudsat and CALIPSO data, *J. Geophys. Res.*, *114*, D00A26, doi:10.1029/2007JD009755.
- Mlawer, E. J., S. J. Taubman, P. D. Brown, M. J. Iacono, and S. A. Clough (1997), Radiative transfer for inhomogeneous atmospheres: RRTM, a validated correlated-k model for the longwave, *J. Geophys. Res.*, *102*(D14), 16,663–16,682, doi:10.1029/97JD00237.
- Morrison, H., and A. Gettelman (2008), A new two-moment bulk stratiform cloud microphysics scheme in the community atmosphere model, version 3 (CAM3). Part I: Description and numerical tests, *J. Clim.*, *21*(15), 3642–3659, doi:10.1175/2008jcli2105.1.
- Park, S., and C. S. Bretherton (2009), The University of Washington shallow convection and moist turbulence schemes and their impact on climate simulations with the Community Atmosphere Model, *J. Clim.*, *22*(12), 3449–3469, doi:10.1175/2008jcli2557.1.
- Peters, M. E., and C. S. Bretherton (2005), A simplified model of the Walker circulation with an interactive ocean mixed layer and cloud-radiative feedbacks, *J. Clim.*, *18*(20), 4216–4234.
- Protat, A., J. Delanoe, E. J. O'Connor, and T. S. L'Ecuyer (2010), The evaluation of CloudSat and CALIPSO ice microphysical products using ground-based cloud radar and lidar observations, *J. Atmos. Ocean. Technol.*, *27*(5), 793–810, doi:10.1175/2009jtecha1397.1.
- Ramanathan, V., R. D. Cess, E. F. Harrison, P. Minnis, B. R. Barkstrom, E. Ahmad, and D. Hartmann (1989), Cloud-radiative forcing and climate: Results from the Earth radiation budget experiment, *Science*, *243*(4887), 57–63.
- Stephens, G. L., et al. (2008), CloudSat mission: Performance and early science after the first year of operation, *J. Geophys. Res.*, *113*, D00A18, doi:10.1029/2008JD009982.
- van Dienenhoven, B., A. M. Fridlind, B. Cairns, and A. S. Ackerman (2014), Variation of ice crystal size, shape, and asymmetry parameter in tops of tropical deep convective clouds, *J. Geophys. Res. Atmos.*, *119*, 11,809–11,825, doi:10.1002/2014JD022385.
- Wielicki, B. A., B. R. Barkstrom, E. F. Harrison, R. B. I. Lee, G. L. Smith, and J. E. Cooper (1996), Clouds and the Earth's Radiant Energy System (CERES): An Earth observing system experiment, *Bull. Am. Meteorol. Soc.*, *77*(5), 853–868.
- Winker, D. M., M. A. Vaughan, A. Omar, Y. X. Hu, K. A. Powell, Z. Y. Liu, W. H. Hunt, and S. A. Young (2009), Overview of the CALIPSO mission and CALIOP data processing algorithms, *J. Atmos. Oceanic Technol.*, *26*(11), 12,310–12,323, doi:10.1175/2009jtecha1281.1.
- Winker, D. M., et al. (2010), THE CALIPSO Mission: A global 3D view of aerosols and clouds, *Bull. Am. Meteorol. Soc.*, *91*(9), 1211–1229, doi:10.1175/2010bams3009.1.
- Yuan, J., and R. A. Houze (2013), Deep convective systems observed by A-Train in the tropical Indo-Pacific region affected by the MJO, *J. Atmos. Sci.*, *70*(2), 465–486, doi:10.1175/jas-d-12-057.1.
- Yuan, J., R. A. Houze, and A. J. Heymsfield (2011), Vertical structures of anvil clouds of tropical mesoscale convective systems observed by CloudSat, *J. Atmos. Sci.*, *68*(8), 1653–1674, doi:10.1175/2011jas3687.1.
- Yuan, J. A., and R. A. Houze (2010), Global variability of mesoscale convective system anvil structure from A-Train satellite data, *J. Clim.*, *23*(21), 5864–5888, doi:10.1175/2010jcli3671.1.
- Zelinka, M. D., and D. L. Hartmann (2010), Why is longwave cloud feedback positive?, *J. Geophys. Res.*, *115*, D16117, doi:10.1029/2010JD013817.
- Zhang, G. J., and N. A. McFarlane (1995), Sensitivity of climate simulations to the parameterization of cumulus convection in the Canadian Climate Center general circulation model, *Atmos.-Ocean*, *33*(3), 407–446.